10.1109/ULTSYM.2015.0305

Dual-Domain Compressed Beamforming for Medical Ultrasound Imaging

Bo Zhang[1], Jean-Luc Robert[2] and Guillaume David[3]
[1]Medisys, Philips Research France, France
[2]Philips Research North America, USA
[3]Biomedical Engineering, Columbia University NY, USA
bo.wang-zhang@philips.com

***Abstract*—In this paper, we propose a novel beamforming approach based on a dual-domain compressed sensing (CS) technique. We model the image as a combination of geometry information and residual details. The beamforming is formulated as depth-dependent optimization problems, solved successively in wavelet domain to capture the overall geometry, and in the image domain to preserve details. With a budget of few iterations, our approach preserves better features and produces less holey-tissue artifacts compared to single-domain reconstructions. Tested on simulated data, CIRS phantom and a cardiac scan, our beamforming requires typically three plane/spherical-wave transmissions to achieve comparable or better image quality than delay-and-sum (DAS) using eleven transmissions. We thus attain a theoretical frame rate over 1KHz at depth of 15cm.**

Keywords*—*Dual-domain compressed sensing, Iterative beamforming, Alternating direction multiplier method

I. Introduction

Compressed sensing (CS) techniques [1][2] have recently drawn great interest in the ultrasound community. Compared to the conventional sampling strategy, CS method is capable of reconstructing signals with many fewer measurements than the Nyquist rate. This is achievable through an efficient sparsity-promoting signal representation that considerably reduces the number of degrees of freedom in the signal estimator. Such property makes CS techniques highly interesting for raw/RF data compression and sampling-rate reduction in ultrasound beamforming, potentially leading to more cost-efficient front-ends (see [3][4][5][6]).

Taking a step further, [7, 8] propose to combine a pulse-echo propagation model into the CS framework, leading to a direct image reconstructor. Compared to the conventional delay-and-sum (DAS) beamformer, this approach produces competitive image quality with a reduced number of transmissions and thus enables higher frame rate.

Despite these encouraging progresses, several image-quality challenges, such as feature preservation and artifact reduction, still underlie current CS-based image reconstructions. Moreover, as an iterative reconstructor, the complexity of CS approaches remains prohibitive for practical imaging. In this work, we try to address improvements in these challenging areas.

We propose herein a novel beamforming approach based on a dual-domain CS technique. It is a known fact that the CS-based beamforming requires a good sparse representation of the image. Along this vein, we find it particularly interesting to model the image as a combination of geometry information and a residue of details. This allows beamforming to be successively carried out in wavelet domain to capture the overall geometry, and in the image domain for preserving features. Numerically, we propose the Alternating Direction Multiplier Method (ADMM) [9] for image reconstruction, as it not only fits our multi-domain strategy, but also produces reasonably accurate results with few iterations.

We evaluate our approach on simulated data, CIRS speckle phantom, and a cardiac scan. We find that our method requires typically only three plane/spherical wave transmissions to achieve comparable or better image quality than DAS using eleven transmissions. Overall, we attain a theoretical frame rate over 1KHz at depth of 15cm. With a budget of few iterations, the approach preserves better features and produces less holey-tissue artifacts, compared to the CS beamforming using a single image-representation domain.

II. Method

A. *Acoustic measurement modeling*

We assume a linear or a phased array transducer (see Fig. 1), transmitting plane wave or diverging wave, and recording acoustic echoes by each of the transducer element (channel).

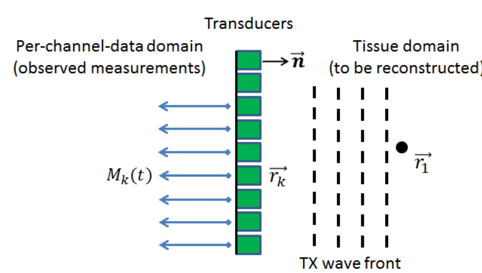

Fig. 1 A linear or phased array transmitting plane-wave pulses and measuring per-channel acoustic-pressure data.

Adopting a linear approximation of the pulse-echo process based on Born's diffraction model [10], the spectrum $\widehat{M}_k(\omega)$ of the per-channel data $M_k(t)$ can be written as a convolution:

$$\widehat{M}_k(\omega) = \int_V f(\omega)\, h_{pe}^{(k)}(\vec{r}_k, \vec{r}_1, \omega) u(\vec{r}_1)\, d\vec{r}_1 \qquad (1)$$

for $k = 1, 2, \dots, N$. Here, $f(\omega)$ is the transfer function of the transducer, $h_{pe}^{(k)}(\vec{r}_k, \vec{r}_1, \omega)$ the pulse-echo transfer function of the k-th transducer element, and u the (unknown) tissue reflexivity to be reconstructed. V, $\vec{r}_1$ and $\vec{r}_k$ respectively denote the probed tissue area, an arbitrary point in V, and the location of the k-th transducer element on the probe surface. In reality, only part of the measurements $\widehat{M}_k$ within the transducer bandwidth are kept, which significantly reduces the number of samples.

We model f by a Gaussian pulse modulated at the transducer frequency. With the plane/spherical-wave emission, h_{pe} can be expressed in closed form (see e.g. [7, 8]). To simplify our notation, the linear operation in (1) can be summarized as

$$\underbrace{\begin{bmatrix} \widehat{M}_1 \\ \widehat{M}_2 \\ \vdots \\ \widehat{M}_N \end{bmatrix}}_{\mathbf{M}} = \underbrace{\begin{bmatrix} G_1 \\ G_2 \\ \vdots \\ G_N \end{bmatrix}}_{\mathbf{G}} u \tag{2}$$

where G_k is the operator regrouping f and $h_{pe}^{(k)}$ as (spatial-variant) convolution kernel in (1). As a consequence, in discrete domain that we consider in the following, $\mathbf{G}$ is represented by a (convolution) matrix.

B. Image reconstruction

Ideally, one needs to inverse (2) to estimate the image u. Due to the ill-conditioning of the inverse problem, conventional CS reconstruction solves a sparsity-promoted optimization problem (3). The sparsity prior is expressed by an l^1-norm within a prescribed basis $\mathbf{W}$ (e.g. wavelets) that is supposed to efficiently represent the image information.

$$\arg\min_{\mathbf{u}} J(\mathbf{u}) = \tfrac{1}{2}\|\mathbf{Gu} - \mathbf{M}\|^2 + \gamma_W \|\mathbf{Wu}\|_1, \ \ \gamma_W > 0 \tag{3}$$

In our case, our image u will be considered as a combination of two components:

$$u = u_g + u_r \tag{4}$$

u_g, or the geometry component, encodes the major structural information in the image. u_r, or the residue component, represents the residual details.

This decomposition explicitly reflects the "multi-layer" nature of medical ultrasound image information. For example, cardiac scans usually includes large structural information such as cardiac walls, and details like valves, thrombus in the chambers, etc. Therefore, the separate modeling in (4) allows us to choose efficient information compression domains according to the nature of the represented information. In our case, we use wavelet bases for sparsifying u_g. For representing the residue u_r, we choose the image pixel basis.

Consequently, our optimization problem is formulated as follows:

$$\arg\min_{\mathbf{u}=[u_g^H, u_r^H]^H} J(\mathbf{u}) = \frac{1}{2}\left\|\mathbf{G}(\mathbf{D}_g + \mathbf{D}_r)\mathbf{u} - \mathbf{M}\right\|^2 + \gamma_W \left\|\mathbf{WD}_g\mathbf{u}\right\|_1 + \gamma_0 \|\mathbf{D}_r\mathbf{u}\|_1 \tag{5}$$

where $\mathbf{u} = \left[u_g^H, u_r^H\right]^H$ concatenates the geometry and residue components into a single vector. $\mathbf{D}_g = [\mathbf{I}, \mathbf{0}]$ and $\mathbf{D}_r = [\mathbf{0}, \mathbf{I}]$ are binary matrices such that $\mathbf{D}_g\mathbf{u} = u_g$ and $\mathbf{D}_r\mathbf{u} = u_r$. $\mathbf{W}$ stands for the wavelet transform matrix. γ_W and γ_0 are positive constants.

It is clear that the optimization in (5) seeks for the best tradeoff between (i) the first term of data fitting using our model (2), and (ii) the second and third terms of l^1-regularization that encode the sparsity prior of the geometry component in the wavelet bases, and of the residue component in the image basis.

C. Numerical solver and implementation

We propose to use ADMM iterative scheme [9] for solving (5). This scheme adopts a divide-and-conquer strategy such that it optimizes alternatively each term of (5) with an augmented Lagrangian relaxation. Hence, the l^1-minimizations in dual domains can be handled independently, which greatly simplifies our implementation.

Moreover, we prefer using undecimated transform of orthogonal wavelets. This makes our wavelet bases $\mathbf{W}$ into a tight frame such that $\frac{1}{F}\mathbf{W}^H\mathbf{W} = \mathbf{I}$. We have the redundancy factor $F = 4^S$ with S the number of wavelet scales. In plain words, the pseudo-inverse of $\mathbf{W}$ boils down to its conjugate transpose up to a constant.

The ADMM scheme is summarized in Table I. Let us denote $\mathbf{B} = \begin{bmatrix}\mathbf{I} & \mathbf{D}_g^H\mathbf{W}^H & \mathbf{D}_r^H\end{bmatrix}^H$, $v_k = \left[v_{(1),k}^H, v_{(2),k}^H, v_{(3),k}^H\right]^H$, and $d_k = \left[d_{(1),k}^H, d_{(2),k}^H, d_{(3),k}^H\right]^H$. Here, $k = 0,1,2,\dots$ indexes the iteration step. At k-th iteration, $v_{(1),k}$, $v_{(2),k}$ and $v_{(3),k}$ record the primal solutions to the three (relaxed) terms of (5) respectively, while $d_{(1),k}$, $d_{(2),k}$ and $d_{(3),k}$ records the corresponding Lagrangian dual variables.

Table I. ADMM numerical algorithm of (5)

Iterate till convergence ($k = 0,1,2,\dots$):		
1.	Solve u_{k+1}	$u_{k+1} = \begin{bmatrix} \frac{1}{F+1}\mathbf{I} & \mathbf{0} \\ \mathbf{0} & \frac{1}{2}\mathbf{I} \end{bmatrix} \mathbf{B}^H(v_k + d_k)$
2.	Solve $v_{(1),k+1}$	$\begin{bmatrix}\mathbf{I}\\\mathbf{I}\end{bmatrix} \mathbf{G}^H\mathbf{G}[\mathbf{I} \quad \mathbf{I}]v_{(1),k+1} + \mu_k v_{(1),k+1} = \begin{bmatrix}\mathbf{I}\\\mathbf{I}\end{bmatrix} \mathbf{G}^H\mathbf{M} + \mu_k(u_{k+1} - d_{(1),k})$
3.	Solve $v_{(2),k+1}$	$v_{(2),k+1} = \mathrm{ST}_{\gamma_W/\mu_k}[\mathbf{WD}_g u_{k+1} - d_{(2),k}]$
4.	Solve $v_{(3),k+1}$	$v_{(3),k+1} = \mathrm{ST}_{\gamma_0/\mu_k}[\mathbf{D}_r u_{k+1} - d_{(3),k}]$
5.	Update d_{k+1}	$d_{k+1} = d_k - \mathbf{B}u_{k+1} + v_{k+1}$

Above, the augmented Lagrangian relaxing parameter $\mu_k > 0$ forms a non-decreasing sequence. $\mathrm{ST}_\beta(v)$ represents the component-wise soft-thresholding operator such that:

$$\mathrm{ST}_\beta(v) \coloneqq \begin{cases} (|v| - \beta)\cdot v/|v| & |v| > \beta \\ 0 & |v| \le \beta \end{cases}$$

In addition, the linear system in step 2 is solved by a few iterations of conjugate gradient descent.

Initially ($k = 0$), our geometry component is set to the back-propagated image $\mathbf{G}^H\mathbf{M}$, while the residue is set to zero.

Then, stages 2, 3 and 4 in Table I find the (relaxed) sub-solutions to the data-fitting term, the geometry component and the residue component of (5), respectively. After updating the dual variables in stage 5, the image solution at the next iteration is found in stage 1 by merging the three sub-solutions. The iteration stops when convergence is reached, or when a prescribed maximum number of iterations is attained.

For a typical transducer of 128 elements, a sensing depth up to 15cm, and a discretized-image pixel size of half of the wavelength, solving (5) on the entire image domain requires a memory size of several hundred gigabytes due to the huge size of the matrix $\mathbf{G}$. To make the solver practically tractable, we propose to partition the image u into (overlapping) stripes of depth of 10mm or 20mm. The numerical solver runs locally on each of the stripes before merging the results:

$$u = \frac{\sum_j W_j u_{[j]}}{\sum_j W_j}$$

$u_{[j]}$ is the solution to the j-th stripe, on which we apply an axial window (e.g. Gaussian) W_j that attenuates the border artifacts. This depth-dependent solver leads to a memory footprint of a few gigabytes, and therefore turns out to be tractable on a common PC.

III. RESULTS AND DISCUSSION

A. *Results on simulated phantom*

We simulate, with Field-II, a linear probe with 128 transducer elements. The probe transmits a single planar-wave pulse and senses a 20mm-by-10mm area ($[60,80] \times [-5,5]\, mm^2$). The area includes a frame of random speckle enclosing 18 isolated diffusers. Their amplitudes range linearly from -50dB to 0dB. The transducer central frequency is 6MHz and the sampling frequency is 40MHz.

The spectral measurements are obtained in the Fourier domain of the per-channel data within the bandwidth. In total, we keep less than 3% of the available Fourier coefficients. We restrict ourselves within a limited time-budget on the number of iterations that does not exceed 20. This corresponds to about 6 min of computation in our Matlab implementation on an Xeon 2.80 GHz PC.

Our γ_0 is set as a fraction to the maximum amplitude in the back-propagation, i.e., $\gamma_0 = 10^{-R_0}\|\mathbf{G}^H\mathbf{M}\|_\infty$ with $R_0 = -2.7$. γ_W is likewise defined (with exponent $R_W = -2.7$) but in the wavelet bands of the back-propagation. We use Haar basis as our wavelets.

In Fig. 2, the dual-domain approach is compared to single wavelet-basis based CS beamforming, single image-basis based CS beamforming and DAS. It can be seen that wavelet-based restoration preserves structural information well but is limited in contrast sensitivity (i.e., up to -35dB). Contrast of isolated diffusers is better preserved using image basis (i.e., up to -47 dB). The tissue frame, however, suffers from holey-tissue artifacts. Dual-domain reconstruction overcomes these limitations and seems to combine the advantages of both domains. Finally, comparing to DAS result, all CS-based methods produce better contrast within the frame. Our display window ranges from -60dB to 0dB.

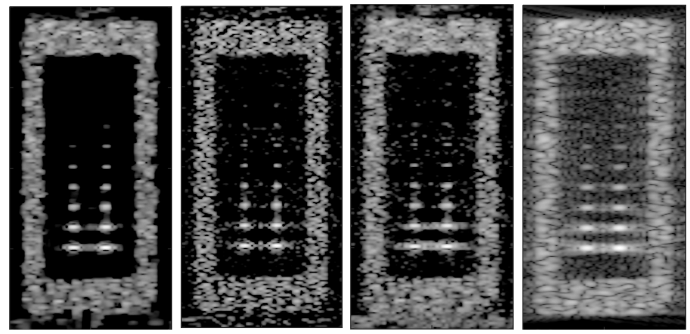

(a) (b) (c) (d)

Fig. 2 Image (20mm x 10mm) reconstructed from a simulated Field-II scan using a linear probe (6 MHz) with a single plane-wave TX. The simulated data consist of a rectangular tissue frame enclosing 18 diffusers of amplitudes ranging from -50 dB to 0 dB. No more than 20 iterations are used in the solvers. (a) CS-beamforming in the wavelet domain; (b) CS-beamforming in the image domain; (c) Dual-domain CS-beamforming; (d) DAS beamformed result.

B. *Results on speckle phantom*

Fig. 3(a) shows our result on the CIRS speckle phantom ($[15,40] \times [-15,15]\, mm^2$) using 3 plane-wave transmissions only (oriented to -5, 0, and 5 degrees). We have set a stripe height of 10mm, no more than 20 iterations, and $R_0 = -2.7$, $R_W = -3.0$.

Compared to DAS with 11 plane-wave transmissions (Fig. 3(b)), the CS-based beamforming shows better axial resolution as well as better lesion contrast in both near and far fields. The improvement is even more significant when comparing to DAS with the same number of transmissions (3 TX, Fig. 3(c)).

We also show the amplitudes of the geometry component u_g and of the residue u_r respectively in Fig. 3(d) and (e). It can be seen that u_g captures the majority of the mostly contrasted signals i.e., cysts, lesions and isolated diffusers. The residual amplitudes on those signals, as well as the remaining speckles in the near field and on the sides are preserved by u_r, which has a porous appearance. Apparently, these results are in consistency with our previous observation on the simulated phantom (Fig. 2).

C. *Results on cardiac scan*

Additionally, we apply our method on cardiac data acquired by a phased-array probe. Our transducer includes 80 elements, and transmits pulses of diverging spherical waves at central frequency 2.6 MHz, focused at 10mm behind the probe surface.

Fig. 4(a) shows our result on a 4-chamber scan with 3 divergent-wave transmissions (oriented to -9, 0, and 9 degrees). The reconstruction is conducted on overlapping stripes of height of 10mm. In each stripe, less than 2% of the total available Fourier coefficients are used. We have set $R_0 = R_W = -2.75$.

Compared to DAS of 11 transmissions in Fig. 4(b), our result provides a better resolution, a comparable contrast in the chambers, and a better contrast in the far field.

In this case, we achieve a theoretical frame rate over 1KHz at depth of 15cm.

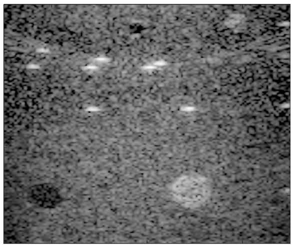

(a)

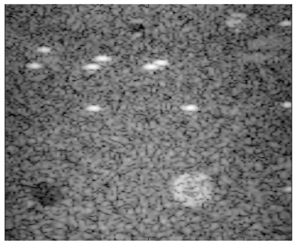

(b)

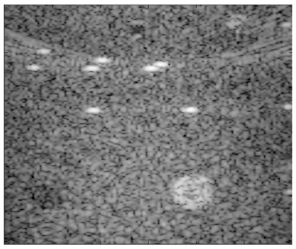

(c)

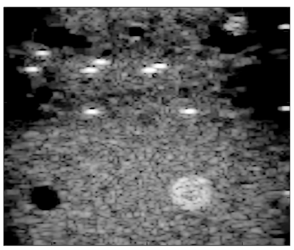

(d)

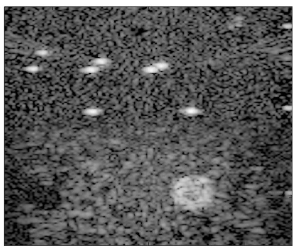

(e)

Fig. 3 CIRS speckle phantom reconstruction using a linear probe (6 MHz). (a) Dual-domain CS-beamforming with 3 transmissions and no more than 20 iterations; (b) DAS with 11 transmissions; (c) DAS with 3 transmissions; (d) the geometry component of the dual-domain solution; (e) the residue component of the dual-domain solution.

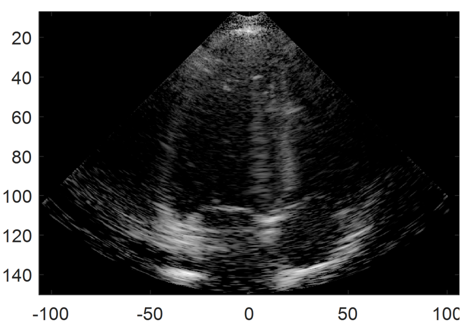

(a)

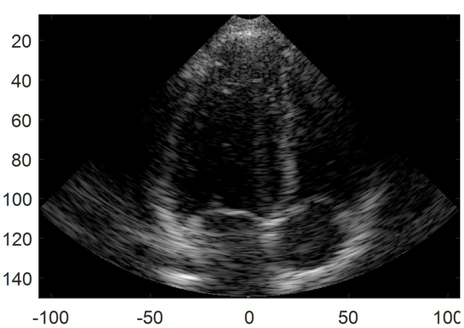

(b)

Fig. 4 Four-chamber scan. (a) Dual-domain CS-beamforming with 3 transmissions and no more than 20 iterations; (b) DAS with 11 transmissions.

IV. CONCLUSION

In this paper, we propose a dual-domain compressed sensing (CS) beamforming technique, based on adapted representations of geometry information and residual details in an ultrasound image. With a budget of few iterations (typically 20), our approach preserves better features and produces less holey-tissue artifacts compared to single-domain approaches. Three plane/spherical-wave transmissions are used in our experiments to achieve comparable or better image quality than delay-and-sum (DAS) using eleven transmissions, attaining a theoretical frame rate over 1KHz at depth of 15cm.

In the future, we will continue our study by focusing on further improvement of the algorithm performance. This would be obtained either by using better iterative numerical schemes, or from a more efficient implementation.

ACKNOWLEDGMENT

The authors would like to thank François Vignon for his valuable comments.

REFERENCES

[1] E. J. Candès, J. K. Romberg, and T. Tao, “Stable signal recovery from incomplete and inaccurate measurements,” Commun. Pur. Appl. Math., vol. 59, no. 8, pp. 1207–1223, 2006.

[2] D. L. Donoho, “Compressed sensing,” IEEE T. Inform. Theory, vol. 52, no. 4, pp. 1289–1306, 2006.

[3] R. Tur, Y. C. Eldar and Z. Friedman, “Innovation rate sampling of pulse streams with application to ultrasound imaging,” IEEE T. Signal Proces., vol. 59, no. 4, pp. 1827–1842, 2011.

[4] C. Quinsac, A. Basarab and D. Kouame, “Frequency domain compressive sampling for ultrasound imaging,” Adv. Acoust. Vib., vol. 2012, 2012.

[5] N. Wagner, Y. C. Eldar and Z. Friedman, “Compressed beamforming in ultrasound imaging,” IEEE T. Signal Proces., vol. 60, no. 9, pp. 4643–4657, 2012.

[6] D. Friboulet, H. Liebgott and R. Prost, “Compressive sensing for raw RF signals reconstruction in ultrasound,” pp. 367–370, IUS 2010.

[7] M. F. Schiffner and G. Schmitz, “Fast pulse-echo ultrasound imaging employing compressive sensing,” pp. 688–691, IUS 2011

[8] M. F. Schiffner and G. Schmitz, “Compensating the combined effects of absoption and dispersion in plane wave pulse-echo ultrasound imaging using sparse recovery,” pp. 573–576, IUS 2013

[9] J. Eckstein and D. Bertsekas, “On the Douglas-Rachford splitting method and the proximal point algorithm for maximal monotone operators,” Math Program., vol. 55, pp. 293–318, 1992

[10] J. A. Jensen, “A model for the propagation and scattering of ultrasound in Tissue”, J. Acoust. Soc. Am., vol. 89, no. 1, pp. 182–190, 1991